

^{210}Pb and composition data of near-surface sediments and interstitial waters evidencing anthropogenic inputs in Amazon River mouth, Macapá, Brazil

José Reinaldo Cardoso Nery^a, Daniel Marcos Bonotto^{b,*}

^aUniversidade Federal do Amapá (UNIFAP), Campus Marco Zero, Rodovia Juscelino Kubitschek, km 2, CEP 68902-280, Macapá, Amapá, Brazil

^bDepartamento de Petrologia e Metalogenia, Universidade Estadual Paulista (UNESP), Câmpus de Rio Claro, Av. 24-A No.1515, C.P. 178, CEP 13506-900, Rio Claro, São Paulo, Brazil

ARTICLE INFO

Article history:

Received 14 March 2010

Received in revised form

19 November 2010

Accepted 25 January 2011

Available online 25 February 2011

Keywords:

Sedimentation rates

Physical weathering

^{210}Pb -chronological method

Amazon River mouth

Anthropogenic influences

ABSTRACT

Activity profiles of excess ^{210}Pb determined in three sediment cores from Amazon River mouth, Macapá city, Brazil, provided the evaluation of sedimentation rates, contributing to a better knowledge of the hydrological conditions in the site that is the capital of Amapá State and is drained by the waters of the huge Amazon River. Chemical data were also determined in the sediments, allowing identify signatures coupled to anthropogenic inputs held in the past in Amapá State. Significant direct relationships between LOI (loss on ignition) and organic matter were found for all sediments profiles. Silica was found to be inversely related to organic matter in the three profiles; its decrease accompanied an increase on the specific surface of the sediments. This relationship was confirmed by a great number of inverse significant correlations among silica and oxides Na_2O , K_2O , CaO , MgO , Al_2O_3 , P_2O_5 , Fe_2O_3 and MnO . It was possible to identify the role of organic matter on adsorption of several oxides in the core sediments profiles. Apparent sediment mass accumulation rates corresponding to values between 450 and 2510 $\text{mg cm}^{-2}\text{yr}^{-1}$ were obtained, and are compatible with the results of others studies. The ^{210}Pb activities in one sampling point suggested the occurrence of anthropogenic inputs related to the initial period of the mining activities conducted in Serra do Navio, Amapá State, for the commercialization of Mn ores. This was reinforced by the abrupt fluctuations in chemical data obtained for the sediments and composition of the interstitial waters occurring there. The Atlantic hurricane activity also appeared to affect the sedimentation rates in the area, as two different values were recorded in each profile.

© 2011 Elsevier Ltd. All rights reserved.

1. Introduction

^{210}Pb is an intermediary member of the natural mass number $(4n + 2)$ ^{238}U decay series that finishes at the stable ^{206}Pb , according to the sequence: ^{238}U (4.49 Ga, α) \rightarrow ^{234}Th (24.1 d, β^-) \rightarrow ^{234}Pa (1.18 min, β^-) \rightarrow ^{234}U (0.248 Ma, α) \rightarrow ^{230}Th (75.2 ka, α) \rightarrow ^{226}Ra (1622 a, α) \rightarrow ^{222}Rn (3.83 d, α) \rightarrow ^{218}Po (3.05 min, α) \rightarrow ^{214}Pb (26.8 min, β^-) \rightarrow ^{214}Bi (19.7 min, β^-) \rightarrow ^{214}Po (0.16 ms, α) \rightarrow ^{210}Pb (22.26 a, β^-) \rightarrow ^{210}Bi (5 d, β^-) \rightarrow ^{210}Po (138 d, α) \rightarrow ^{206}Pb .

^{222}Rn emanating from land surfaces is responsible for ^{210}Pb present in the atmosphere, whose removal occurs by precipitation. The atmospheric ^{210}Pb returning to the earth's surface has been commonly referred to as unsupported (excess) ^{210}Pb , whereas the ^{210}Pb resulting from the decay of ^{238}U within rocks, soils, minerals

and sediments has been termed supported (*in situ* produced) ^{210}Pb (Baskaran and Naidu, 1995).

^{210}Pb is a particle-reactive radionuclide readily removed from the water column through adsorption onto particulate matter and their coatings (organic or Fe–Mn oxides) (DeMaster et al., 1986). Numerous studies have utilized ^{210}Pb data as chronometer for sediment accumulation and mixing in lakes, estuarine, marsh, and coastal areas (for a comprehensive review, see Appleby and Oldfield, 1992), since they provide a reliable dating method over the last 100–150 years. In general, there are difficulties on obtaining ^{210}Pb concentration data that are above the detection limit in river sediments, a situation commonly verified in Brazil, where the ^{210}Pb -derived chronology has been mainly developed at lakes and coastal areas (Godoy et al., 1998). Additionally, the radioactive disequilibrium in the U decay series generally caused by ^{222}Rn loss from sediments has to be considered, since it would cause a depletion of supported ^{210}Pb , leading to non-equilibrium conditions between ^{226}Ra and ^{210}Pb (Ravichandran et al., 1995).

A comprehensive study of a variety of radionuclide tracers, including ^{210}Pb , was coupled with geochemical investigations and

* Corresponding author. Tel.: +55 19 35262825; fax: +55 19 35249644.

E-mail addresses: jrnery@unifap.br (J.R.C. Nery), danielbonotto@yahoo.com.br (D.M. Bonotto).

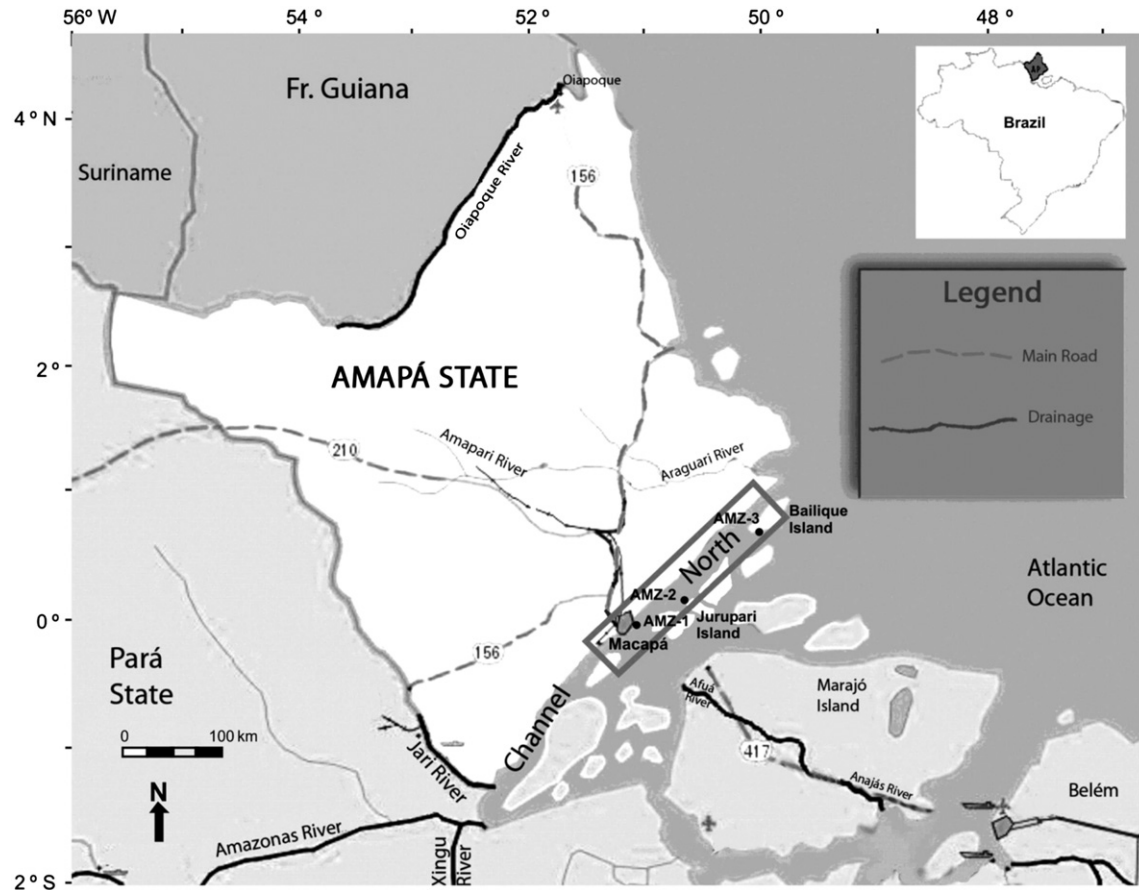


Fig. 1. Location of Macapá city in Amapá State, Brazil, and of the sampling points for interstitial waters and sediments profiles in Amazon River mouth.

with sedimentary and physical oceanographic measurements to elucidate processes and their characteristic time scales at the mouth of the Amazon River. This was undertaken as part of A Multidisciplinary Amazon Shelf SEDiment Study (*AmasSeds*) where four cruises aboard the R/V *Columbus Iselin* were designed from August 1989 to November 1991 to correspond to variations in the river discharge, wind stress and flow rates of the North Brazil Current (NBC). The study provided a rare opportunity to detail processes occurring in that highly energetic environment and along the coastal area of Amapá State, Brazil, and many data were published, increasing substantially the knowledge of the Amazon continental shelf (for instance, Allison et al., 1995; Dukat and Kuehl, 1995; Jaeger and Nittrouer, 1995; Kineke and Sternberg, 1995; Kuehl et al., 1995, 1996; Moore et al., 1995, 1996; Nittrouer et al., 1995, 1996; Smoak et al., 1996).

This paper presents a complete new ^{210}Pb and composition dataset in near-surface sediments and interstitial waters collected at the Amazon River mouth. The sampling sites were different of those utilized during the *AmasSeds* program, bringing relevant information on possible processes occurring there. This is because the data on the chemical composition of sediments and interstitial waters were coupled with ^{210}Pb data in order to provide a scenario that evidences anthropogenic inputs occurring in the area. These supplies are possibly related to the initial period of the mining activities held in Serra do Navio, Amapá State, for the commercialization of Mn ores, and have not been pointed out by previous investigations held there.

2. General features of the area investigated

The Amazon area spreads over 9 countries, but almost 67% of its surface area (~ 5 million km^2) is inserted within the Brazilian

territory in nine states where only about 7.6% of the Brazilian population is living there (IBGE, 2007). The Amazon River starts flowing in the Andes Cordillera at Peru (5600 m of altitude), intercepts a short part of south Colombia and flows through the northern portion of Brazil in the west–east direction until its discharge in the Atlantic Ocean between Amapá and Pará States. It receives the following names, along its 6840 km of extension: Lloqueta, Apurimac, Ene, Tambo, Ucayali, Solimões and Amazonas. It is the largest in world either in extension or amount of water discharged ($\sim 200,000 \text{ m}^3/\text{s}$ during the rainy season) (Domínguez, 2004). The total number of affluents corresponds to about 7000 along its flow, where its discharge is ~ 60 times higher than that of the Nile River, the second largest in world. The width of the Amazon River is variable, ranging from 13 to 50 km in Manaus city (Amazonas State, Brazil), depending on the dry and rainy season. It is narrower (1800 m) and deeper (50 m) at Óbidos city (Pará State in Brazil), where the discharge is $200,000 \text{ m}^3/\text{s}$. The average water level high is 10 m, reaching 16 m in the rainy season. The amount of sediments released into Atlantic Ocean is huge, circa 800 billion tons per year (Brandini, 2005).

Different types of waters have been documented in the Amazon basin, many of them named according to their color, for instance, Rio Negro (black water), Rio Branco (white water), Rio Claro (clear water) (Furch, 1984; Furch and Junk, 1997). The colors of the waters have been related to specific conditions of the catchment areas and according to Sioli (1950) and Furch and Junk (1997) three basic types of river waters have been recognized: (a) white water rivers, as the Amazon River, which are rich in suspended silt and dissolved minerals, carried from the Andes and Andean foothills, having a near-neutral pH; (b) black water rivers, which are black *in situ*,

Table 1
Grain size analysis of the sediments.

Depth range (cm)	Total weight, TW (%)	Dry weight, DW (%)	Cumulated dry weight/area (g/cm ²)	Weight (%) ^a							Moisture (%)	Porosity ^c ϕ (%)	
				GRA ^b	VCS ^b	CRS ^b	MES ^b	FIS ^b	VFS ^b	CSI ^b			MSI ^b
Profile AMZ-1 (Latitude – 00°00'06"S; Longitude – 51°03'37"W)													
0–10	9.90	8.63	11.30	0	0	43.46	44.75	1.57	9.44	0.66	0.13	33.9	57.7
10–20	10.01	10.55	25.13	0	0	38.75	34.38	4.94	20.82	0.89	0.23	20.1	40.0
20–30	9.83	10.14	38.41	0	0	2.17	20.60	55.67	19.57	1.82	0.16	21.7	42.4
30–40	9.97	10.08	51.61	0	0	0.87	23.86	49.01	24.51	1.64	0.11	23.4	44.7
40–50	10.41	10.62	65.52	0	0	0	0.86	34.12	62.41	2.28	0.33	22.7	43.7
50–60	10.22	10.29	79.00	0	0	0	1.18	55.20	42.12	1.21	0.28	23.7	45.1
60–70	10.10	10.21	92.37	0	0	0	1.98	33.42	63.12	1.33	0.16	23.4	44.7
70–80	10.59	10.67	106.34	0	0	0	2.37	48.49	47.61	1.37	0.15	23.6	45.0
80–90	9.29	9.21	118.41	0	0	0	1.51	51.82	44.35	2.18	0.14	24.8	46.7
90–100	9.67	9.60	130.99	0	0	0	1.58	46.34	50.83	1.11	0.13	24.7	46.6
Profile AMZ-2 (Latitude – 00°11'40"N; Longitude – 50°37'13"W)													
0–10	8.87	8.61	10.44	0.07	0.46	0.69	29.97	45.67	19.96	2.93	0.25	31.9	55.4
10–20	9.84	8.83	21.15	0.07	0.71	2.16	34.09	38.49	22.15	2.19	0.13	37.1	61.0
20–30	9.74	9.00	32.10	0.11	1.39	2.20	26.77	47.30	20.88	1.28	0.07	35.2	59.0
30–40	9.34	9.10	43.11	0.13	1.11	2.33	32.06	45.54	17.68	1.09	0.06	31.7	55.1
40–50	10.47	11.25	56.75	0.00	0.16	0.33	22.21	67.52	9.16	0.58	0.04	24.7	46.4
50–60	10.13	10.25	69.17	0.33	1.16	2.34	30.94	35.57	28.29	1.30	0.08	29.1	52.1
60–70	10.20	9.93	81.22	0.18	1.48	2.72	2.66	31.42	59.67	1.74	0.12	31.7	55.2
70–80	10.42	10.90	94.43	0.07	0.60	1.29	0.89	28.51	64.85	3.64	0.14	26.7	49.1
80–90	10.15	10.88	107.62	0.02	0.36	0.91	0.64	49.15	47.42	1.44	0.05	24.9	46.7
90–100	10.84	11.25	121.27	0.00	0.10	0.10	0.26	33.16	64.54	1.80	0.04	27.3	49.8
Profile AMZ-3 (Latitude – 00°54'13"N; Longitude – 50°00'01"W)													
0–10	10.55	10.61	15.15	0	0	0	0.03	62.82	32.71	3.78	0.65	23.8	45.3
10–20	10.05	10.32	29.88	0	0	0.02	0.05	72.13	23.45	3.30	1.06	22.2	43.0
20–30	9.94	10.05	44.23	0	0.02	0.02	0.03	86.53	11.48	1.51	0.42	23.3	44.7
30–40	10.05	9.97	58.46	0	0.05	0.08	0.08	58.91	36.86	2.97	1.04	24.8	46.6
40–50	10.05	10.24	73.08	0	0.09	0.12	0.06	84.54	13.91	1.10	0.17	22.7	43.9
50–60	9.18	8.68	85.48	0	0.18	0.13	0.35	62.18	35.56	1.40	0.20	28.3	51.2
60–70	9.97	10.03	99.81	0	0.18	0.14	0.08	67.93	30.88	0.61	0.18	23.7	45.1
70–80	9.70	9.63	113.55	0	0.05	0.03	0.03	82.90	15.74	0.75	0.50	24.8	46.7
80–90	10.03	9.98	127.79	0	0.06	0.06	0.05	84.59	14.04	0.87	0.32	24.6	46.4
90–100	10.47	10.48	142.75	0	0.05	0.05	0.03	85.30	13.43	0.74	0.40	24.2	45.8

^a Calculated from the raw weight of each sediment size fraction.

^b Udden (1898) scale (in mm) and Wentworth (1922) classification: GRA = granule (>2.0 mm), VCS = very coarse sand (2.0–1.0 mm), CRS = coarse sand (1.0–0.5 mm), MES = medium sand (0.5–0.25 mm), FIS = fine sand (0.25–0.125 mm), VFS = very fine sand (0.125–0.063 mm), CSI = coarse silt (0.063–0.031 mm), MSI = medium silt (<0.031 mm).

^c $\phi = TW - DW/TW + DW (\rho_1/\rho_2 - 1)$, where ρ_1 = water density (1 g/cm³) and ρ_2 = sediments density (2.65 g/cm³). According to Argollo (2001).

present high levels of humic and fulvic acids, leached from podzolic soils, have acidic pH, are poor in ions and present high transparency compared to the white water rivers; and (c) clear water rivers, drained from highly weathered Tertiary sediments, that have pH varying from acidic to neutral, are low in dissolved minerals and present high transparency but may be greenish.

The area of investigation in this paper is situated in the border of Amapá and Pará States, in the Amazon region at the northern part of Brazil (Fig. 1). It lies between the coordinates: latitude – 1°02' N and 0°29' S; longitude – 49°21' W and 51°11' W. The region comprises the Channel North at the estuarine portion of Amazon River and includes Macapá city, the capital of Amapá State. The Channel North in the area exhibits a huge water volume that is discharged into Atlantic Ocean along 320 km of coastal line (Brandini, 2005).

2.1. Some anthropogenic inputs due to the mining activities of Mn ores

Amapá State possesses an abundant hydrological net in the Amazon area, where the hydrographic basin of Araguari River is the most important, occupying about one third of the State surface area (~42,710 km²) (Bárbara et al., 2005). The Araguari River has an extension of 300 km, starts flowing southwards in Serra Tumucumaque and, then, moves eastwards until its discharge in Atlantic Ocean between the coordinates: latitude – 0°30' N and 1°30' N; longitude – 51°00' W and 52°30' W (Bárbara et al., 2005). Highly

energetic conditions are found in the estuarine mouth of this river, forming tidal bores (pororocas) and surface gravity waves (1–2 m height) that are produced by the seasonally variable trade-winds (Allison et al., 1995). Silveira (1998) utilized multi-temporal analysis for investigating the sediments supply along the Amapá State coast and found that the areas between the right margin of Araguari River and the Bailique islands are subjected to accumulation/accretion processes. The sampling point AMZ-3 (Fig. 1) is situated in this zone and, despite the extensive contribution of the Amazon River, Silveira (1998) pointed out that the sources of sediments supply remain unclear, where anthropogenic inputs can also take place.

Amapari River is the main tributary of Araguari River, which drains Serra do Navio situated 150 km northwest from Macapá city where it was located an important Mn mining area. Two principal Mn ores were identified in that site (Scarpelli, 2003): a) primary, consisting of manganiferous marble layers and b) secondary (manganese oxides and hydroxides masses), formed by weathering of the primary ore. The mineral assemblage coupled to these ores and adjacent rocks involves the presence of carbonate (rhodochrosite-MnCO₃), silicates [spessartine-Mn²⁺Al₂(SiO₄)₃; tephroite-Mn²⁺(SiO₄)], sulfides (Fe, Cu, Zn, Co, Ni), oxides/hydroxides [psilomelane; pyrolusite-MnO₂; lithiophorite-(Al,Li)MnO₂(OH)₂; limonite-FeO(OH).nH₂O; goethite- α -Fe³⁺O(OH); gibbsite-Al₂O₃], clays, silica and others secondary minerals (Scarpelli, 2003).

The Brazilian company ICOMI (*Indústria e Comércio de Minérios*) mined and commercialized Mn ores from Serra do Navio between 1957 and 1997, where the manganiferous ore blocks were removed,

Table 2
Chemical analyses of the sediments cores sampled at Amazonas River mouth, Amapá State, Brazil.

Depth Range (cm)	SiO ₂ (%)	Na ₂ O (%)	K ₂ O (%)	CaO (%)	MgO (%)	Al ₂ O ₃ (%)	P ₂ O ₅ (%)	Fe ₂ O ₃ (%)	MnO (%)	TiO ₂ (%)	LOI ^a (%)	OM ^b (%)
Profile AMZ-1												
0–10	84.82	1.05	1.52	0.69	0.14	6.10	0.09	2.94	0.04	0.66	1.97	0.58
10–20	84.44	1.16	1.54	0.75	0.19	6.26	0.09	2.94	0.04	0.71	1.88	0.55
20–30	82.68	1.34	1.82	0.78	0.34	6.91	0.09	3.08	0.04	0.66	2.24	0.75
30–40	81.98	1.28	1.78	0.80	0.36	7.40	0.10	3.00	0.05	0.64	2.62	0.90
40–50	82.95	1.34	1.77	0.81	0.32	6.84	0.09	3.05	0.04	0.63	2.16	0.69
50–60	82.81	1.32	1.77	0.82	0.30	6.82	0.10	3.05	0.05	0.66	2.30	0.88
60–70	82.90	1.28	1.71	0.82	0.32	6.77	0.10	3.15	0.05	0.69	2.21	0.69
70–80	82.75	1.23	1.69	0.82	0.34	6.81	0.11	3.20	0.05	0.69	2.31	0.80
80–90	83.25	1.29	1.68	0.85	0.32	6.64	0.11	3.06	0.05	0.68	2.07	0.58
90–100	82.95	1.30	1.90	0.90	0.30	6.76	0.10	3.04	0.04	0.74	2.02	0.54
Mean	83.11	1.26	1.72	0.81	0.30	6.73	0.10	3.07	0.05	0.67	2.19	0.70
Profile AMZ-2												
0–10	78.67	1.09	1.62	0.97	0.77	8.52	0.12	4.31	0.08	1.30	2.56	1.03
10–20	73.40	1.27	2.02	1.05	1.01	11.27	0.12	4.50	0.09	0.85	4.43	1.34
20–30	75.15	1.23	1.96	0.99	0.94	10.61	0.11	4.10	0.08	0.85	4.00	1.41
30–40	75.64	1.24	1.96	0.98	0.87	10.48	0.11	4.15	0.07	0.74	3.76	1.46
40–50	80.43	1.24	1.83	0.92	0.68	8.68	0.09	3.19	0.04	0.60	2.30	0.53
50–60	77.71	1.24	1.88	1.00	0.85	9.34	0.11	3.81	0.06	0.85	3.14	0.80
60–70	75.39	1.25	1.92	1.03	0.94	10.08	0.11	4.20	0.08	0.83	4.15	1.08
70–80	79.64	1.17	1.77	0.94	0.74	8.50	0.10	3.65	0.05	0.72	2.75	0.56
80–90	80.45	1.09	1.67	0.90	0.72	8.34	0.10	3.35	0.05	0.74	2.59	0.63
90–100	80.59	1.10	1.64	0.98	0.75	7.79	0.10	3.82	0.05	0.80	2.37	0.53
Mean	77.71	1.19	1.83	0.98	0.83	9.36	0.11	3.91	0.07	0.83	3.21	0.94
Profile AMZ-3												
0–10	86.33	0.89	1.30	0.65	0.44	6.04	0.08	2.44	0.07	0.48	1.31	0.43
10–20	83.76	0.97	1.45	0.78	0.55	6.67	0.09	3.25	0.07	0.73	1.69	0.55
20–30	83.63	1.00	1.54	0.75	0.52	6.57	0.08	3.40	0.06	0.54	1.88	0.51
30–40	82.94	1.10	1.60	0.75	0.56	6.92	0.08	3.38	0.06	0.51	2.09	0.63
40–50	84.11	1.03	1.53	0.74	0.52	6.45	0.08	3.16	0.06	0.54	1.75	0.62
50–60	77.08	1.13	1.80	0.88	0.67	8.68	0.13	5.43	0.10	0.50	3.61	0.81
60–70	84.07	1.00	1.49	0.75	0.52	6.65	0.08	2.94	0.06	0.52	1.91	0.53
70–80	83.98	1.03	1.55	0.76	0.55	6.56	0.08	2.99	0.06	0.55	1.90	0.43
80–90	84.82	1.00	1.48	0.73	0.52	6.26	0.08	2.78	0.06	0.49	1.78	0.24
90–100	85.44	0.92	1.37	0.75	0.50	5.99	0.08	2.69	0.06	0.57	1.64	0.41
Mean	83.62	1.01	1.51	0.75	0.54	6.68	0.09	3.25	0.07	0.54	1.96	0.52

^a LOI = loss on ignition.

^b OM = organic matter.

crushed, sieved and washed for clays removal (Scarpelli, 2003). Tailings piles and ponds/lakes were extensively generated in that area due to the mining activities. The high rainfall, air temperature and water acidity in Serra do Navio area are natural conditions that have favored the rock decomposition and formation of weathering profiles reaching more than 100 m depth there (Scarpelli, 2003). They are also able to promote strong reactions with the disturbed geologic materials through oxidation reactions, releasing sulfate-rich and carbonate-rich fluids that can migrate into ground and surface water sources. Thus, such emissions occasionally could reach the Araguari River mouth (Fig. 1).

3. Experimental

3.1. Sampling campaign

The fieldwork was undertaken utilizing small boats (when necessary) for reaching the sampling sites, whose coordinates are shown in Table 1. The first sampling point (AMZ-1) was located in the urban area of Macapá city, the second (AMZ-2) in its rural area (Jurupari islands) and the third (AMZ-3) close to the Araguari River mouth (Bailique islands). The samples were collected at the Amazon River margins, during periods of low tides when the sediments had been exposed at the surface (0-m isobath).

The study area (Fig. 1) is not the same of those focused in previous researches held on the Amazon shelf by the *AmasSeds* project that directed its efforts on a large area extending from the south side of the Amazon River mouth along shore to the Brazil-French Guiana border, and from the shoreline across the topset,

foreset and bottomset regions of the active sub-aqueous delta to relict transgressive sands on the outer shelf (Nittrouer et al., 1995). The findings of that study have opened up an appreciation of the complex interaction that takes place between the river water sediments and the ocean water. The area studied in this paper focused the near-surface environment that provided sediments and information representative of the riverine systems until the mouth.

A 1–1.1 m long PVC tube (7.5 cm in diameter) was driven into the sediments, each profile being cut in 10 cm thick slices that were transferred to polyethylene bags. After recovering the cores, the interstitial water migrated into the bores and was also manually collected for chemical analyses. The water samples were stored in 2 L polyethylene bottles previously cleaned by an appropriate treatment (acid washing with 10% nitric acid and rinsing with Milli Q water) that was finished on rinsing by the same water sampled.

3.2. Analytical methods

All bags containing the sediments and polyethylene bottles with the water samples were stored in iceboxes and transported to the laboratory. The water content of each sediments section was determined after drying at 60 °C for about 24 h for organic matter preservation and minimal loss of volatile compounds. The dried sediments were classified in terms of color according to the Munsell (1975) chart, disaggregated with a porcelain mortar, homogenized, weighted, and separated into aliquots for physical, chemical and radiochemical analysis. Aliquots for granulation analysis were pulverized using an agate mortar and pestle, sieved through a screen

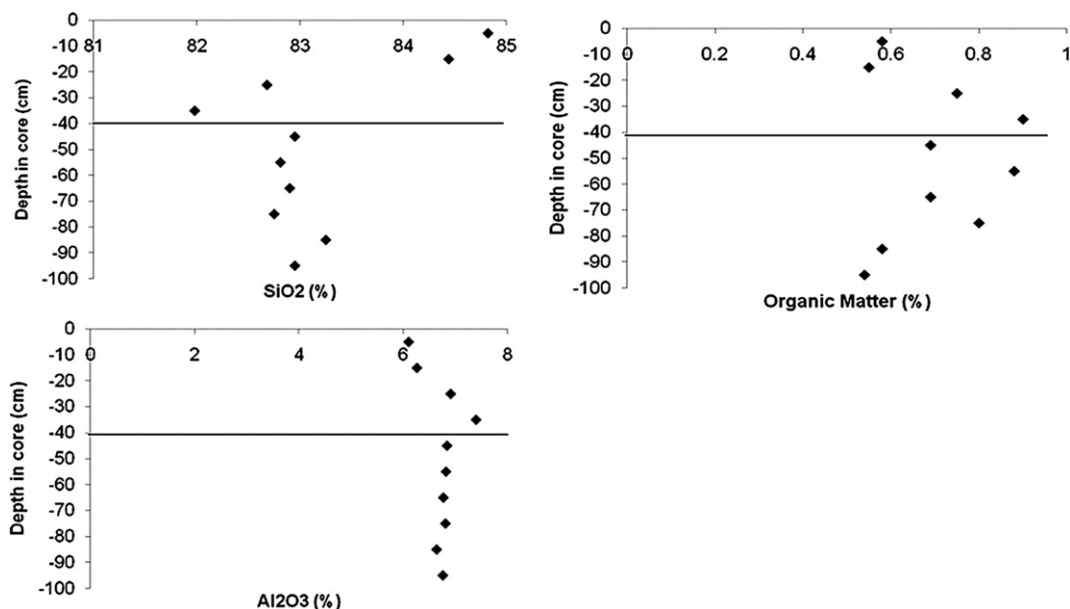


Fig. 2. The data for SiO₂, organic matter and Al₂O₃ in sediments collected at the Amazon River mouth, Amapá State, plotted against depth in core AMZ-1.

net defined by the Udden (1898) scale, and classified according to Wentworth (1922).

The major oxides in the sediments were determined in one 5 g aliquot by the X-ray fluorescence method. The chemical balance (in percentage) also supplied data on the loss on ignition (LOI), as the measurements involved weight loss of the samples after their burning at selected temperatures. Organic matter (OM) was evaluated by spectrophotometry (Hach, 1992) held in a solution obtained after adding potassium dichromate and sulfuric acid to 1-g powdered aliquot not submitted to digestion. Organic carbon was oxidized to carbon dioxide with a parallel reduction of hexavalent chromium to trivalent chromium and an accompanying color change from orange to green read at 610 nm (Hach, 1992). The porosity (ϕ) of each aliquot was calculated as described by Argollo (2001) from the water content, typical water density (1 g cm^{-3}) and average density of 2.65 g cm^{-3} for predominating minerals (quartz, feldspars and kaolinite).

Standard methods (APHA, 1989) were utilized to analyze the water samples, for instance, potentiometry (for measuring pH and conductivity), atomic absorption (for quantifying Na), spectrophotometry (for measuring K, Ca, Mg, sulfate, nitrate), titration (for evaluating bicarbonate), ion selective electrode and potentiometry (for evaluating chloride), and dryness and weighing (for calculating the dry residue).

²¹⁰Pb in the river sediments was determined by the quantification of its granddaughter ²¹⁰Po. Homogeneous portions of dried samples from each core were used, with a 0.5 g aliquot of these powders being digested in a mixture of HCl + HNO₃ at ~60 °C. The solution was brought to dryness, and the dry residue was dissolved with 8 M HCl to a volume of 15 mL. A known amount (0.2 mL; activity = 40 dpm/mL) of ²⁰⁹Po spike was added at the beginning of each digestion to assess ²¹⁰Po recovery. To each sample in a 50-mL Teflon beaker, 5 mL of 20% hydroxylamine hydrochloride and 2 mL of 25% sodium citrate solution were added, and the pH was adjusted to 2 with concentrated ammonia solution (Flynn, 1968). Polonium was plated onto a copper disc (2.5-cm diameter) and measured by conventional alpha spectroscopy according to the procedure described by Bonotto and Lima (2006).

To obtain information about the parent-supported (*in-situ* produced) ²¹⁰Pb, measurements of equivalent uranium, eU

(²¹⁴Bi = ²²⁶Ra), were performed on the same homogeneous portions of dried samples from each core used for ²¹⁰Po analysis. Aliquots ranging from 49 to 67 g were submitted to γ -ray spectrometry through a 2" × 2" NaI(Tl) scintillation detector and a 2048-channels multichannel analyzer provided by Ortec Ace 2K hardware controlled by MAESTRO software. The system was calibrated in energy and for ²¹⁴Bi readings using the method reported by Duarte and Bonotto (2000), where the eU concentration data in ppm were converted to dpm/g, as $1 \mu\text{g U} = 0.746 \text{ dpm}$.

4. Results and discussion

4.1. Texture and chemical composition of the sediments

Tables 1 and 2 report the results obtained for all sediments analyzed. The sediment cores exhibited similar color patterns along the profiles, dominating the clear brownish gray color (Munsell, 1975). The porosity of the sediments ranged between 40 and 61%, and the two highest values in profile AMZ-2 corresponded to an accentuated presence of organic matter in the porous media (1.3–1.4%). The high porosity values facilitated the accumulation of interstitial water, allowing its easy sampling in the bores investigated.

The sediments presented variable grain size, with dominance of fine sand (250–125 μm) to very fine sand (125–63 μm) along the profiles. However, the fine sand dominated the entire profile AMZ-3, whereas the same was not found in profiles AMZ-1 and AMZ-2 where frequently occurred alternated dominance between fine sand and very fine sand. Sediment cores that were collected from the Amazon shelf by a 3-m long, square gravity (kasten) corer and analyzed by Dukat and Kuehl (1995) consisted predominantly of clay-sized particles, less than 1% sand (>63 μm), and up to 10% coarse silt (31–63 μm). Studies held by Allison et al. (1995) on sediment cores obtained from nine field excursions to the Amapá coast during 1989–1991 utilized a Sedigraph model 5100 to analyze the grain size of the mud fraction (<63 μm) and an automated 180-cm settling column to examine the sand-size particles. The sand characteristics from the three northern river sandbodies were identical (unimodal, very well sorted and fine to very fine sands), but the Araguari River sandbody exhibited a mean grain size

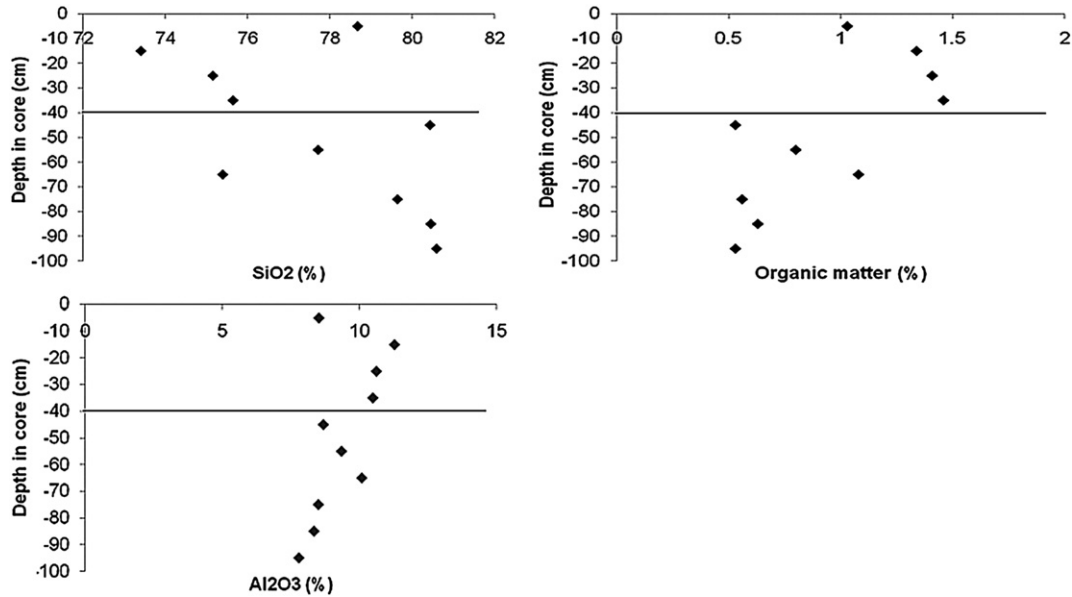


Fig. 3. The data for SiO₂, organic matter and Al₂O₃ in sediments collected at the Amazon River mouth, Amapá State, plotted against depth in core AMZ-2.

corresponding to very fine sand, that is not the same of that dominating the profile AMZ-3 (Table 1).

Loss on Ignition (LOI) expresses the organic matter + adsorbed water + water in crystal lattices and fluid inclusions + CO₂ of carbonates + SO₂ of sulfides. LOI ranged from 1.3 to 4.4% in the sediment cores (Table 2) and because it is a parameter associated with organic matter, there are significant relationships between LOI and organic matter in all profiles analyzed (AMZ-1: $r = 0.92$; AMZ-2: $r = 0.85$; AMZ-3: $r = 0.72$).

Beyond modifying the bulk density and porosity of soils and sediments, organic matter also influences their specific surface (area per mass, often expressed in m²/g), since 1% of organic matter in porous matrices may cause an increase of the specific surface of about 7 m² (Kiehl, 1977). Consequently, other parameters are also

significantly affected. Cation exchange capacity, cation adsorption, and percentage of water retention in soils/sediments, in general, increase during rising of the specific surface. Silica is the major oxide of all analyzed profiles, reaching mean concentration values higher than 78% in the profiles (Table 2). However, the SiO₂ content decreases in accordance with the increase of organic matter in all profiles (AMZ-1: $r = -0.84$; AMZ-2: $r = -0.98$; AMZ-3: $r = -0.98$).

The decrease in SiO₂ concentration is expected to be accompanied by an increase in the specific surface of the sediments, implying on an enhanced cation exchange/adsorption capacity. Such expectance was confirmed by a great number of inverse significant correlations in all profiles: silica and Na₂O (AMZ-1: $r = -0.83$; AMZ-2: $r = -0.71$; AMZ-3: $r = -0.82$); silica and K₂O (AMZ-1: $r = -0.82$; AMZ-2: $r = -0.85$; AMZ-3: $r = -0.93$); silica

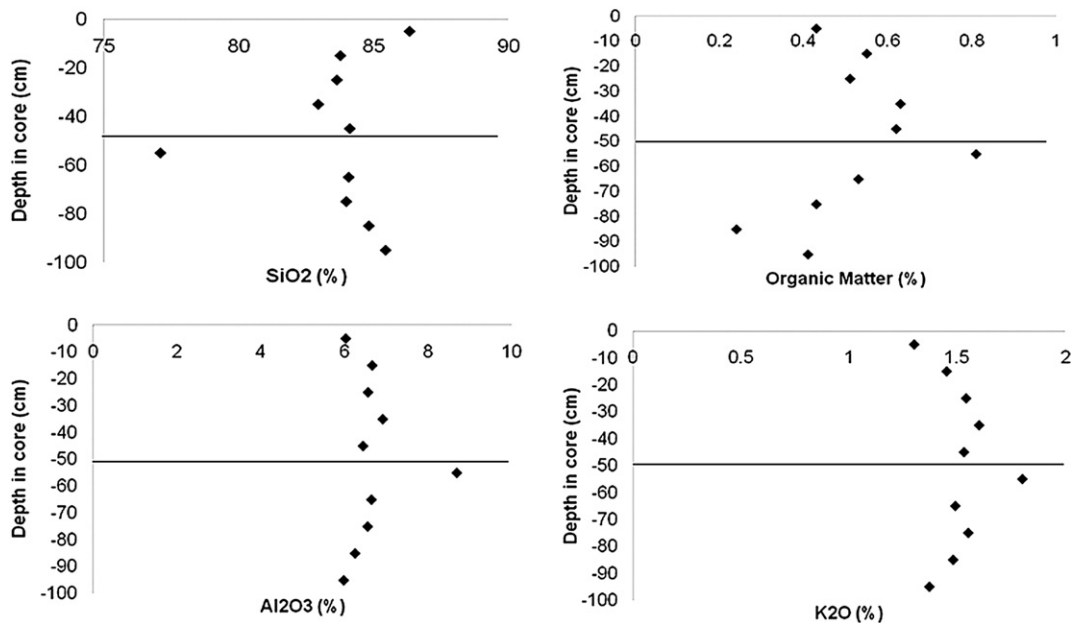


Fig. 4. The data for SiO₂, organic matter, Al₂O₃ and K₂O in sediments collected at the Amazon River mouth, Amapá State, plotted against depth in core AMZ-3.

and CaO (AMZ-1: $r = -0.64$; AMZ-2: $r = -0.83$; AMZ-3: $r = -0.91$); silica and MgO (AMZ-1: $r = -0.96$; AMZ-2: $r = -0.97$; AMZ-3: $r = -0.95$); silica and Al_2O_3 (AMZ-1: $r = -0.97$; AMZ-2: $r = -0.97$; AMZ-3: $r = -0.99$); silica and Fe_2O_3 (AMZ-1: $r = -0.58$; AMZ-2: $r = -0.81$; AMZ-3: $r = -0.99$); silica and MnO (AMZ-2: $r = -0.88$; AMZ-3: $r = -0.82$); silica and P_2O_5 (AMZ-2: $r = -0.73$; AMZ-3: $r = -0.92$).

It is also possible identify the organic matter role on the adsorption of several oxides/elements in the studied core sediments profiles, as evidenced by the following direct significant correlations: LOI and Na_2O (AMZ-2: $r = 0.71$; AMZ-3: $r = 0.80$); LOI and K_2O (AMZ-2: $r = 0.86$; AMZ-3: $r = 0.91$); LOI and CaO (AMZ-2: $r = 0.79$; AMZ-3: $r = 0.89$); LOI and MgO (AMZ-1: $r = 0.73$; AMZ-2: $r = 0.97$; AMZ-3: $r = 0.93$); LOI and Al_2O_3 (AMZ-1: $r = 0.89$; AMZ-2: $r = 0.95$; AMZ-3: $r = 0.97$); LOI and Fe_2O_3 (AMZ-2: $r = 0.72$; AMZ-3: $r = 0.97$); LOI and MnO (AMZ-1: $r = 0.62$; AMZ-2: $r = 0.81$; AMZ-3: $r = 0.81$); LOI and P_2O_5 (AMZ-2: $r = 0.62$; AMZ-3: $r = 0.91$).

Allison et al. (1995) investigated the sand mineralogy along the 350-km shoreline adjacent to the Amazon River mouth and found that quartz is the primary mineral component (78–89%) with variable quantities of lateritic grains (2–12%), mica (0–6%), feldspar (2–4%), heavy minerals (2–6%) and minor constituents (<1%). The laterite content was low in Amazon River sand and relatively high in Amapá rivers sand, indicating that the rivers of Amapá State drain source areas with intense chemical weathering. Mica was concentrated in the sandbodies of Araguari River and the analysis of the heavy-mineral assemblage in them revealed that biotite was the major constituent.

4.2. Chemical composition of the sediments and anthropogenic inputs

The concentration data of some selected constituents in the sediment cores AMZ-1, AMZ-2 and AMZ-3 are plotted against depth in Figs. 2–5, which also display the depth of occurrence of an abrupt fluctuation in their abundance and excess ^{210}Pb activity (Section 4.4).

The compounds plotted against depth in sampling points AMZ-1 and AMZ-2 were silica, organic matter and Al_2O_3 , as shown in Figs. 2 and 3. The trends verified in the break zone corresponded to those already described in Section 4.1, i.e. a decreasing SiO_2 content corresponded to an increasing on the organic matter concentration,

and vice-versa. The organic matter role on the metals adsorption in sediment profiles AMZ-1 and AMZ-2 is illustrated by the trends verified between the Al_2O_3 content and organic matter concentration in the break zone: both decrease after crossing the boundary layer at ~ 40 cm depth.

The break in the chemical composition of the sediments in sampling point AMZ-3 occurred in a deeper zone (~ 50 cm) relatively to AMZ-1 and AMZ-2 (Fig. 4). The Al_2O_3 content and organic matter concentration in AMZ-3 increased after crossing the boundary layer (Fig. 4), contrarily to found in AMZ-1 (Fig. 2) and AMZ-2 (Fig. 3). The silica fluctuation across the break layer in AMZ-3 (Fig. 4) as well exhibited an opposite trend to that found in AMZ-1 (Fig. 2) and AMZ-2 (Fig. 3). However, the direct relations between the Al_2O_3 content and organic matter concentration and the inverse relations between SiO_2 and organic matter are maintained after crossing the break zones of all profiles (AMZ-1, AMZ-2 and AMZ-3).

One notable aspect occurring in profile AMZ-3 relatively to profiles AMZ-1 and AMZ-2 is the accentuated jump on the concentrations of SiO_2 , Al_2O_3 and organic matter after reaching ~ 50 cm depth. Such strong fluctuation also occurred in profile AMZ-3 for others constituents like K_2O , CaO, MgO, P_2O_5 , Fe_2O_3 and MnO (Figs. 4 and 5). All these oxides are widely spread in mining tailings associated to the Mn ores from Serra do Navio, which were produced during the removal, crushing, sieving and washing of the manganese ore blocks. Thus, their leaching to Amapari River and further transport to the major draining system could reach the Araguari River mouth at the Amapá State coast. The sampling point AMZ-3 (Fig. 1) is closely situated between the right margin of Araguari River and the Bailique islands in an area subjected to accumulation/accretion processes (Allison et al., 1995) that is favorable to receive occasional emissions occurring in the riverine systems.

One plausible explanation for the non-accentuated fluctuation in the Na_2O concentration like verified for others oxides in profile AMZ-3 (Fig. 5) may be related to the high solubility of sodium in surface waters. Goldich (1938) evaluated the chemical weathering of granitic gneiss from southern Minnesota, USA, verifying the occurrence of rapid loss of plagioclase and biotite, and slower removal of K-feldspar and quartz. Such finding allowed Goldich (1938) to show that the susceptibilities of the rock-forming silicate minerals to weathering are related to their position in Bowen's reaction series (i.e. dependence on temperature of crystallization

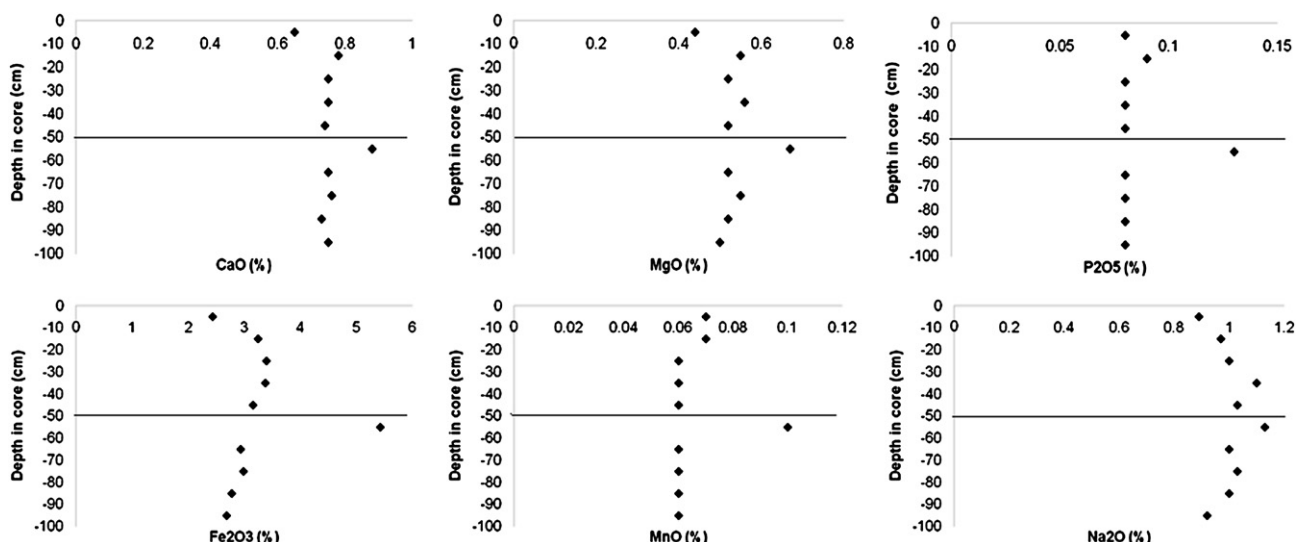


Fig. 5. The data for CaO, MgO, P_2O_5 , Fe_2O_3 , MnO and Na_2O in sediments collected at the Amazon River mouth, Amapá State, plotted against depth in core AMZ-3.

Table 3

Results of the analyses of interstitial water samples collected at the Amazon River mouth, Amapá State, Brazil, and comparison with different types of waters occurring in the Amazon basin.

Parameter	Sampling point ^a			Amazon basin ^b		
	AMZ-1	AMZ-2	AMZ-3	Negro River	Solimões/Amazon River	Forest streams
pH	6.6	6.9	7.2	5.1 ± 0.6	6.9 ± 0.4	4.5 ± 0.2
Conductivity (μS/cm)	50	124	254	9 ± 2	57 ± 8	10 ± 3
Dry Residue (mg/L)	25	62	127	n.a.	n.a.	n.a.
Cl ⁻ (mg/L)	9.3	10.0	11.7	1.7 ± 0.7	3.1 ± 2.1	2.2 ± 0.4
NO ₃ ⁻ (mg/L)	0.3	1.2	2.5	n.a.	n.a.	n.a.
HCO ₃ ⁻ (mg/L)	13	42	114	n.a.	n.a.	n.a.
SO ₄ ²⁻ (mg/L)	<1	<1	230	n.a.	n.a.	n.a.
Ca ²⁺ (mg/L)	33.6	38.4	54.1	0.21 ± 0.07	7.2 ± 1.6	0.04 ± 0.03
Mg ²⁺ (mg/L)	24.3	13.6	24.3	0.11 ± 0.04	1.1 ± 0.2	0.04 ± 0.02
Na ⁺ (mg/L)	3.9	8.6	6.9	0.38 ± 0.12	2.3 ± 0.8	0.22 ± 0.06
K ⁺ (mg/L)	1.3	1.8	1.1	0.33 ± 0.11	0.9 ± 0.2	0.15 ± 0.11
Ionic Strength (×10 ⁻³)	4.0	3.8	9.3	n.a.	n.a.	n.a.

^a This paper.

^b According to Furch (1984) and Furch and Junk (1997); n.a. = not available.

from a magma), in which olivine and Ca-plagioclase are considered most susceptible followed by pyroxene, hornblende, biotite, and Na-plagioclase (Faure, 1991). The Goldich (1938) proposition was based on fine observations that the weathering processes promote rapid losses of Na and Ca oxides, whereas the decrease in the concentrations of the K and Mg oxides occurs slowly with time.

Therefore, the strong fluctuations verified ~50 cm depth in profile AMZ-3 for the concentrations of SiO₂, Al₂O₃, K₂O, CaO, MgO, P₂O₅, Fe₂O₃ and MnO is compatible with the occurrence of anthropogenic inputs coupled to the mining activities involving Mn ores at Serra do Navio.

4.3. Chemical composition of the interstitial waters and anthropogenic inputs

Table 3 summarizes some hydrochemical data for river and stream waters of the Amazon basin and also reports the results obtained for the interstitial water samples collected at the three cores studied in this paper. All the pH values are within the range of the reported values for the Solimões/Amazon River, whose waters exhibit a conductivity equivalent to that found for the interstitial waters of the sampling point AMZ-1. The conductivity in AMZ-3 is 5 times higher than in AMZ-1 and is linked to the more elevated values of the sodium, calcium, sulfate, nitrate, bicarbonate and dry residue contents in AMZ-3. The insertion of the analytical data in a partial Piper (1944) diagram (Fig. 6) allows identifying different hydrochemical facies for the waters studied, i.e. magnesium-chloride (AMZ-1), calcium-bicarbonate (AMZ-2) and calcium-sulfate (AMZ-3). Thus, different sources/processes may be responsible for this variability.

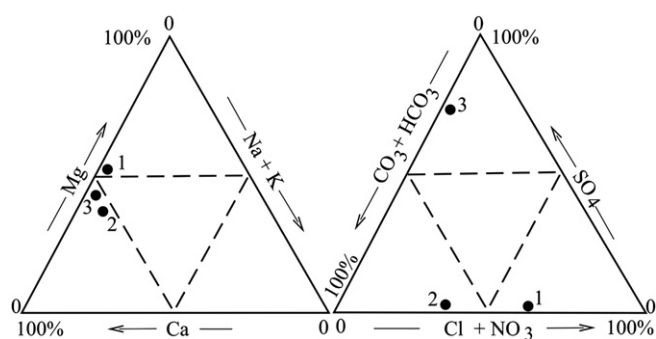


Fig. 6. The data for major cations and anions in waters collected at the Amazon River mouth, Amapá State, plotted on a partial Piper (1944) diagram (1 = AMZ-1; 2 = AMZ-2; 3 = AMZ-3).

The comparison of the data reported in Table 3 for major cations and chloride in waters of the Solimões/Amazon River with the results obtained for interstitial waters collected at the Amazon River mouth indicates higher values in the three sampling points (AMZ-1, AMZ-2 and AMZ-3). Because of their proximity to urban and rural zones, in principle, it could be admitted some contribution of anthropogenic inputs to the riverine water chemistry. On the other hand, it also would be possible some influence of the ocean waters since a number of processes act energetically in the area, including the density driven circulation caused by the huge freshwater discharge, the North Brazil Current, strong semidiurnal tides, and the northeast trade winds (Kineke and Sternberg, 1995).

Additionally, one very important finding is the elevated concentration of sulfate and bicarbonate in sampling point AMZ-3 relatively to AMZ-1 and AMZ-2. Its location favors the possibility of some influence of the ocean waters in that site, which could enhance the dissolved sulfate and bicarbonate contents. However, it is well known that chloride is the most conservative species and most dominant anion in sea water, reaching almost 20 g/L (Faure, 1991). But it only increases from 9.3 mg/L in AMZ-1–11.7 mg/L in AMZ-3, which is negligible.

Therefore, another input source, other than sea water, appears to affect the water chemistry in AMZ-3. A plausible mechanism consists on the strong reactions with the disturbed geologic materials through oxidation reactions in Serra do Navio area that are naturally favored by the high rainfall, air temperature and water acidity. As a consequence, emissions of sulfate-rich and carbonate-rich fluids are promoted, which can migrate into ground and surface waters, occasionally reaching the Araguari River mouth. Such process could justify the enhanced concentrations of sulfate and bicarbonate in the interstitial water at profile AMZ-3 (Table 3). It is also compatible with the strong fluctuations verified ~50 cm depth in profile AMZ-3 for the concentrations of SiO₂, Al₂O₃, K₂O, CaO, MgO, P₂O₅, Fe₂O₃ and MnO, as pointed out in Section 4.2. Thus, the enhanced dissolved sulfate and bicarbonate contents in the interstitial water at profile AMZ-3 also agree with possible anthropogenic inputs coupled to the mining activities involving Mn ores at Serra do Navio.

4.4. Radionuclides data and fluctuations in the excess ²¹⁰Pb activity concentration

The radiochemical data in all core sediments are given in Table 4. The eU (²²⁶Ra) activity concentration values range from 0.01 to 1.5 dpm/g and, in principle, could be used as an estimate of the parent-supported (*in-situ* produced) ²¹⁰Pb. However, ²²⁶Ra reaches ²¹⁰Pb after four α-decays and two β⁻-decays, producing the noble

Table 4
Radiochemical data of the sediments cores sampled at the Amazon River mouth, Amapá State, Brazil.

Depth range (cm)	eU ^a (dpm g ⁻¹)	Total ²¹⁰ Pb activity, ^a ²¹⁰ Pb _T (dpm g ⁻¹)	Supported ²¹⁰ Pb activity, ^b ²¹⁰ Pb _s (dpm g ⁻¹)	Excess ²¹⁰ Pb activity, ^c ²¹⁰ Pb _{xs} (dpm g ⁻¹)	ln (²¹⁰ Pb _{xs}) (dpm g ⁻¹)	Deposition time (years)	Deposition year
Profile AMZ-1							
0–10	0.714 ± 0.038	1.011 ± 0.074	0.114	0.897	-0.11	16	1990
10–20	0.872 ± 0.036	0.573 ± 0.118	0.139	0.434	-0.83	35	1971
20–30	0.635 ± 0.035	0.192 ± 0.020	0.102	0.090	-2.41	53	1953
30–40	0.717 ± 0.038	0.341 ± 0.046	0.115	0.226	-1.49	72	1934
40–50	0.727 ± 0.036	1.064 ± 0.070	0.116	0.948	-0.05	85	1921
50–60	0.337 ± 0.025	0.568 ± 0.060	0.054	0.514	-0.66	97	1909
60–70	0.078 ± 0.013	0.297 ± 0.032	0.012	0.285	-1.26	109	1897
70–80	0.244 ± 0.020	0.343 ± 0.044	0.039	0.304	-1.19	122	1884
80–90	0.809 ± 0.039	0.374 ± 0.066	0.129	0.245	-1.41	133	1873
90–100	1.217 ± 0.050	0.302 ± 0.046	0.195	0.107	-2.23	145	1861
Profile AMZ-2							
0–10	1.539 ± 0.053	2.039 ± 0.228	0.246	1.793	0.58	23	1983
10–20	0.954 ± 0.044	0.668 ± 0.204	0.153	0.515	-0.66	47	1959
20–30	1.415 ± 0.053	0.690 ± 0.108	0.226	0.464	-0.77	71	1935
30–40	1.012 ± 0.043	0.309 ± 0.134	0.162	0.147	-1.92	96	1910
40–50	0.370 ± 0.026	1.078 ± 0.250	0.059	1.019	0.02	103	1903
50–60	0.713 ± 0.038	0.635 ± 0.108	0.114	0.521	-0.65	109	1897
60–70	0.236 ± 0.022	0.720 ± 0.072	0.038	0.682	-0.38	116	1890
70–80	0.441 ± 0.028	0.645 ± 0.180	0.071	0.574	-0.55	122	1884
80–90	0.540 ± 0.032	0.442 ± 0.296	0.086	0.356	-1.03	129	1877
90–100	0.255 ± 0.020	0.517 ± 0.082	0.041	0.476	-0.74	136	1870
Profile AMZ-3							
0–10	0.160 ± 0.016	0.730 ± 0.096	0.026	0.704	-0.35	9	1997
10–20	0.182 ± 0.018	0.679 ± 0.148	0.029	0.650	-0.43	17	1989
20–30	0.013 ± 0.004	0.450 ± 0.114	0.002	0.448	-0.80	26	1980
30–40	0.494 ± 0.027	0.416 ± 0.080	0.079	0.337	-1.09	34	1972
40–50	0.629 ± 0.032	0.669 ± 0.090	0.101	0.568	-0.56	40	1966
50–60	0.250 ± 0.019	0.847 ± 0.236	0.040	0.807	-0.21	45	1961
60–70	0.109 ± 0.014	0.883 ± 0.146	0.017	0.866	-0.14	50	1956
70–80	0.100 ± 0.013	0.464 ± 0.094	0.016	0.448	-0.80	56	1950
80–90	0.463 ± 0.026	0.686 ± 0.098	0.074	0.612	-0.49	62	1944
90–100	0.106 ± 0.013	0.417 ± 0.140	0.017	0.400	-0.92	68	1938

^a Analytical uncertainty corresponding to 1σ standard deviation.

^b ²¹⁰Pb_s = 0.16 (eU).

^c ²¹⁰Pb_{xs} = ²¹⁰Pb_T - ²¹⁰Pb_s.

gas ²²²Rn in this decay succession. Since some of the ²²²Rn produced escapes from sediments to the surrounding water and air, only a fraction of Rn atoms formed in the solid phase will contribute to the generation of ²¹⁰Pb.

The ²²²Rn-loss from soil and rock surfaces is greatly dependent of the surface area as demonstrated in several investigations. For instance, laboratory time-scale experiments were conducted by Bonotto and Andrews (1997) on Carboniferous Limestone gravels from the Mendip Hills area, England, with the purpose of evaluating the release of ²²²Rn to the water phase. The specific surface areas of the samples were 4.14 and 1.69 cm² g⁻¹, which provided, respectively, values of 112.3 and 28.2 dpm for the radon released, demonstrating the relationship between surface area and radon release. Another set of laboratorial experiments was conducted by Bonotto and Andrews (1999) on soils from the Mendip Hills area and the results obtained for those derived from Carboniferous Limestone were: total surface area of 3.57 and 1.82 m² and ²²²Rn activity of 430.7 and 137.6 dpm, respectively, again showing the relationship between surface area and radon release. The radon release in those experiments was computed from the emanation coefficient or emanating efficiency (E) by the following equation (Wanty et al., 1992):

$$E = \frac{(^{222}\text{Rn})_{\text{fluid}}}{(^{222}\text{Rn})_{\text{fluid}} + (^{222}\text{Rn})_{\text{solid}}} \quad (1)$$

Where: (²²²Rn)_{fluid} is the radon dissolved in water and (²²²Rn)_{solid} is the radon produced in rocky or soil matrices from ²²⁶Ra.

Bonotto and Caprioglio (2002) also realized laboratory time-scale experiments with different samples of sedimentary rocks in order to evaluate the radon release and an average value of E = 0.84 was obtained from eqn. (1), indicating that only 16% of the ²²²Rn generated by ²²⁶Ra decay contributes to the production of ²¹⁰Pb. Such factor was successfully utilized by Bonotto and Lima (2006) in two sediment cores from Corumbataí River basin, São Paulo State, Brazil, where activity profiles of excess ²¹⁰Pb combined with chemical data provided new insights on the reconstruction of historical inputs of anthropogenic constituents. This was possible due to the similarity of the grain sizes, which imply on equivalents surface area and ²²²Rn-loss. The same factor will be used in this paper by the same reasons, meaning that only 16% of the ²²²Rn generated by ²²⁶Ra produces ²¹⁰Pb. Thus, the supported ²¹⁰Pb, ²¹⁰Pb_s, can be calculated from the equation:

$$^{210}\text{Pb}_s = 0.16(\text{eU}) \quad (2)$$

Where: eU is the equivalent uranium (²¹⁴Bi = ²²⁶Ra). The results obtained are given in Table 4.

The ²¹⁰Po activity concentration measured by alpha spectrometry corresponded to the total ²¹⁰Pb activity, ²¹⁰Pb_T. The values obtained are reported in Table 4 and they were found disregarding the time Δt elapsed since the finishing of the plating procedure and ending of the alpha counting (often between 24 and 60 h). The excess ²¹⁰Pb activity, ²¹⁰Pb_{xs}, was calculated as the difference between total and supported activities, i.e. ²¹⁰Pb_{xs} = ²¹⁰Pb_T - ²¹⁰Pb_s.

The excess ²¹⁰Pb activity ranged between 0.09 and 1.8 dpm/g, as reported in Table 4. The excess ²¹⁰Pb activity is plotted against

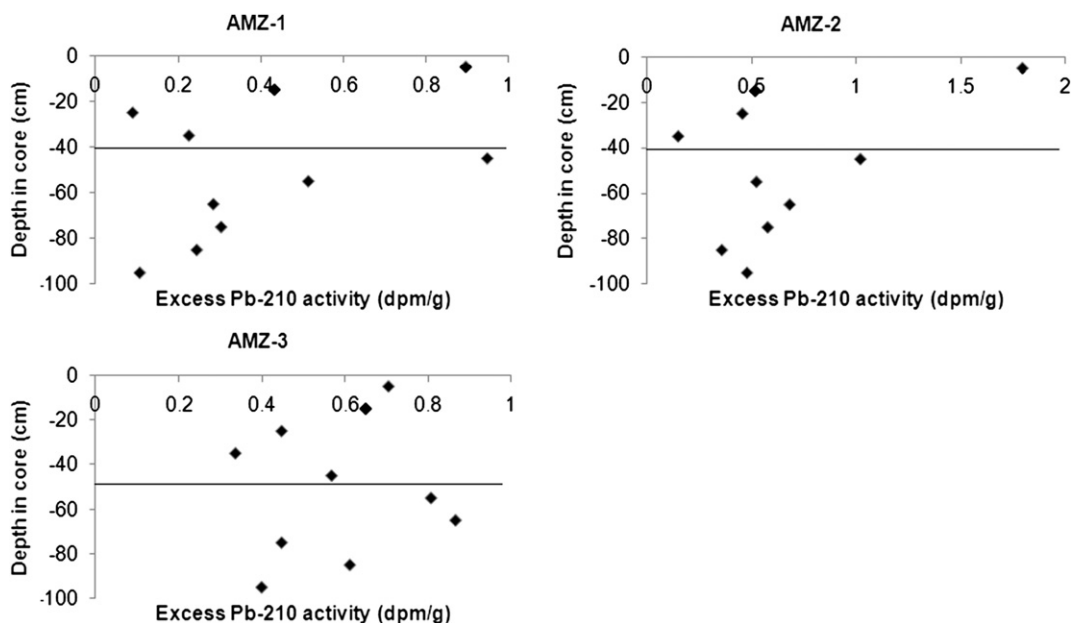


Fig. 7. The data for excess ²¹⁰Pb activity in sediments collected at the Amazon River mouth, Amapá State, plotted against depth in cores AMZ-1, AMZ-2 and AMZ-3.

depth in Fig. 7, which shows that all profiles display a significant break in ²¹⁰Pb activity, though the exact depth varies from core AMZ-3 relatively to cores AMZ-1 and AMZ-2.

4.5. Sedimentation rates and anthropogenic inputs

During the *AmasSeds* program, several sampling schemes were used and the aliquots separation for ²¹⁰Pb analysis was not the same in the cores, which were characterized every 1 cm, 2 cm, 5 cm or 10 cm, depending on the purpose of each study. Despite the 10-cm sampling interval adopted in this study is not adequate to resolve some ²¹⁰Pb cycles, it provides rough estimates of sedimentation rates according to the CIC (constant initial concentration) of unsupported/excess ²¹⁰Pb model (Appleby and Oldfield, 1978). Such model assumes the occurrence of sediments compaction and that the flux of ²¹⁰Pb from the water to the sediments is constant or that the flux of the solids coming from the atmosphere and brought by rainfall is constant. This implies that the concentration of unsupported ²¹⁰Pb in the initial sediments bed is constant. Another condition for the applicability of this model is that the sedimentation rate has to be constant during the investigated period of time, producing an exponential diminution of the ²¹⁰Pb activity in accordance with the depth of the sediments column. The excess ²¹⁰Pb activity at any layer z of the sediment column, ²¹⁰Pb_{xs(z)}, is (Baskaran and Naidu, 1995):

$$^{210}\text{Pb}_{\text{xs}(z)} = ^{210}\text{Pb}_{\text{xs}(0)} e^{-\lambda_{210}t} \tag{3}$$

Where: ²¹⁰Pb_{xs(0)} represents the excess ²¹⁰Pb activity at the sediment–water interface, λ₂₁₀ is the ²¹⁰Pb decay constant (0.0311 yr⁻¹), and t is the deposition time (age, in years). This equation can be simplified and rewritten as:

$$\ln^{210}\text{Pb}_{\text{xs}(z)} - \ln^{210}\text{Pb}_{\text{xs}(0)} = (-\lambda_{210}f^{-1})w \tag{4}$$

Where: the cumulated dry weight per unit area (g cm⁻²), w, is related to the deposition time according to the expression t = wf⁻¹ (f is the sediment mass flux in g cm⁻² yr⁻¹).

When ln ²¹⁰Pb_{xs(z)} is plotted against the cumulated dry weight per unit area, w, the resulting ²¹⁰Pb profile will be linear, with slope -λ₂₁₀f⁻¹. The sediment mass flux, f, may then be determined from the mean slope of the profile, using the least-squares fit procedure (Baskaran and Naidu, 1995). The ln (²¹⁰Pb_{xs}) data obtained in this study (Table 4) were plotted against the cumulated dry weight per unit area in Fig. 8. Two different sedimentation rates were obtained in each profile, which are linked to the breaks in ²¹⁰Pb activities shown in Fig. 7. The straight lines were statistically significant (95% confidence level) and the mass accumulation rates were higher in the deeper portion of the profiles.

The deposition time (in years) has been calculated on dividing the cumulated dry weight per unit area by the sediment mass accumulation rate, and is plotted against depth in Fig. 9. The expected deposition year for each sediments layer (Table 4) was estimated considering the sampling year (2006) and the water–sediments interface at the uppermost layer as reference for establishing the chronology.

The sediment mass accumulation rates determined in this paper are compared in Table 5 with some reported values either at a local or global scale. Two different sedimentation rates in the same profile were also reported in others sites like in Chapala Lake (Mexico) and Conceição Lake (Rondônia State, Brazil), indicating that the trends verified in the area here studied are not unique. Additionally, high rates exceeding 1000 mg cm⁻²yr⁻¹ are not exclusive of the Amazon River mouth or of Amazon lakes situated at Rondônia and Pará states in Brazil as it also occurred in Ibitinga Creek situated at Rio Claro municipality in São Paulo State. However, the most prominent rate corresponding to 2510 mg cm⁻²yr⁻¹ was found in profile AMZ-3 in the Amazon River mouth and such finding agrees with the expected importance of this system to sediments supplies to the ocean.

The average linear sedimentation rate can also be evaluated on dividing the total thickness of the sediments column by the deposition time at the deepest layer. In this case, it ranges from 0.42 to 1.76 cm yr⁻¹ that is compatible with values estimated at others sites (Godoy et al., 1998; Moreira-Turcq et al., 2004; Vergotti, 2008) and also agrees with some values reported during the execution of

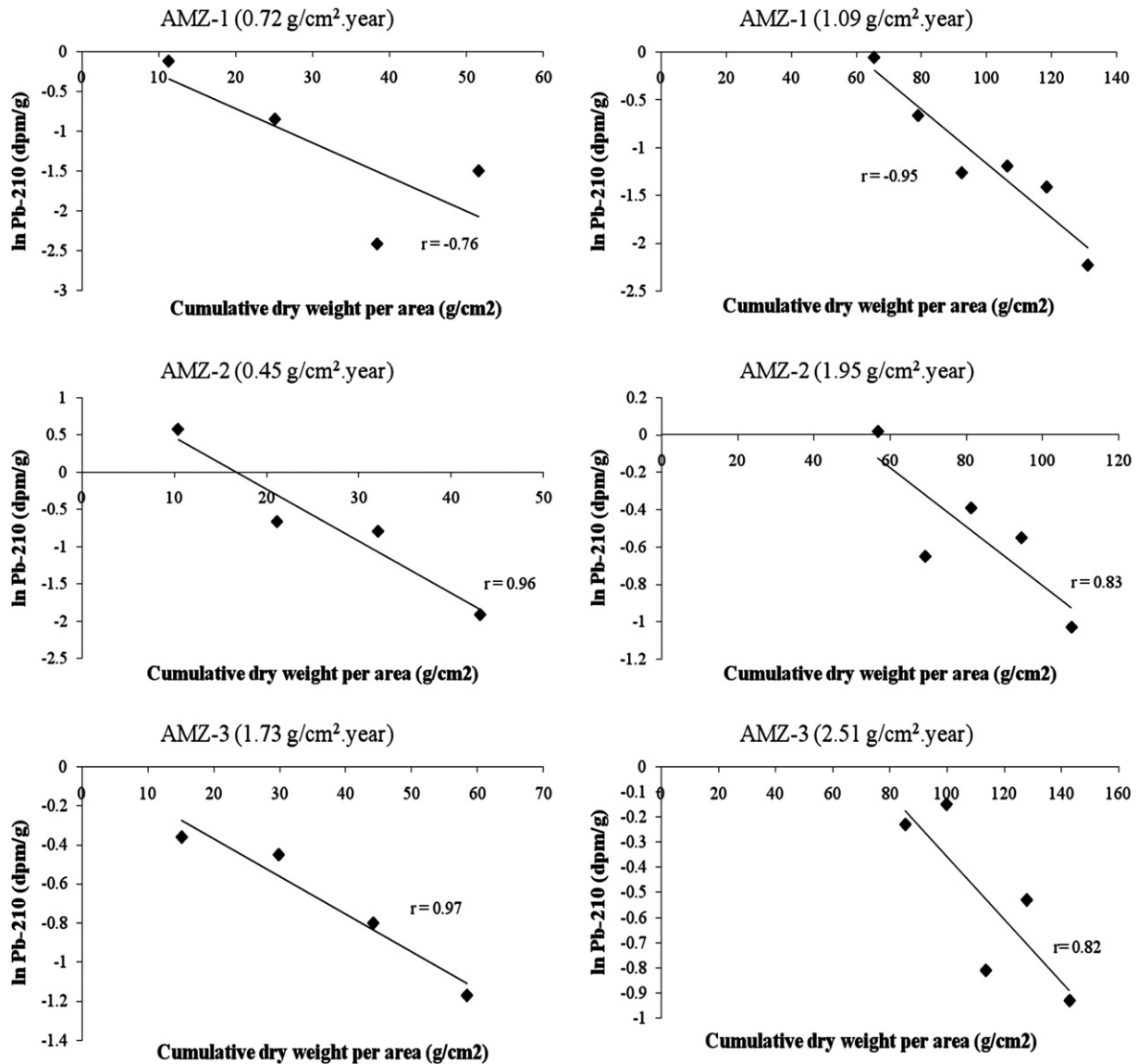


Fig. 8. Excess ^{210}Pb vs. cumulative dry mass relationships in sediment cores AMZ-1, AMZ-2 and AMZ-3 at Amazon River mouth, Amapá State, Brazil.

the *AmasSeds* program, for instance, 0.24–2.0 cm yr^{-1} in several cores analyzed by Allison et al. (1995).

The rates and deposition times obtained ~ 50 cm depth in profile AMZ-3 may be compared with the initial period of the mining activities held in Serra do Navio, Amapá State, by the Brazilian company ICOMI (*Indústria e Comércio de Minérios*) for the commercialization of Mn ores. They were realized between 1957 and 1997, with the production reaching values of 600,000–760,000 tons of mined manganese from 1957 to 1960 (Drummond and Pereira, 2007). This epoch approximately coincides with the deposition times obtained ~ 50 cm depth in profile AMZ-3 by the ^{210}Pb method. It is well known that the beginning of the mining activities involved the presence of many labors and several machines for performing the extensive operations that involved the cutting and removal of the rocky blocks, crushing, sieving and washing for clays removal. These actions are highly polluting to the environment, affecting the hydrological resources and, consequently, the Al_2O_3 , K_2O , CaO , MgO , P_2O_5 , Fe_2O_3 and MnO concentrations at ~ 50 cm depth in core AMZ-3. Therefore, the adoption of the steady-state condition requested by the application of the ^{210}Pb

method to profile AMZ-3 provided an useful approach for explaining the abrupt increase in the concentration of several constituents in sediments ~ 50 cm depth, as well the enhanced dissolved sulfate and bicarbonate contents in the interstitial water.

4.6. Abrupt breaks in the sedimentation rates

Different characteristic zones on the Amazon shelf have been identified by the *AmasSeds* project from ^{210}Pb data (Dukat and Kuehl, 1995; Kuehl et al., 1995, 1996; Jaeger and Nittrouer, 1995; Moore et al., 1996; Smoak et al., 1996): near-surface zones of uniform and of non-steady-state (quasi-cyclic) fluctuations in ^{210}Pb activity, zones of logarithmic decrease in excess ^{210}Pb activity, and zones of low uniform ^{226}Ra -supported ^{210}Pb activity. Accumulation rates have been calculated from the slope of excess ^{210}Pb in the zones of logarithmic decrease, whereas ^{210}Pb cyclicity has produced non-steady-state activity profiles, limiting the use of ^{210}Pb as a geochronometer (Dukat and Kuehl, 1995; Jaeger and Nittrouer, 1995; Kuehl et al., 1995, 1996).

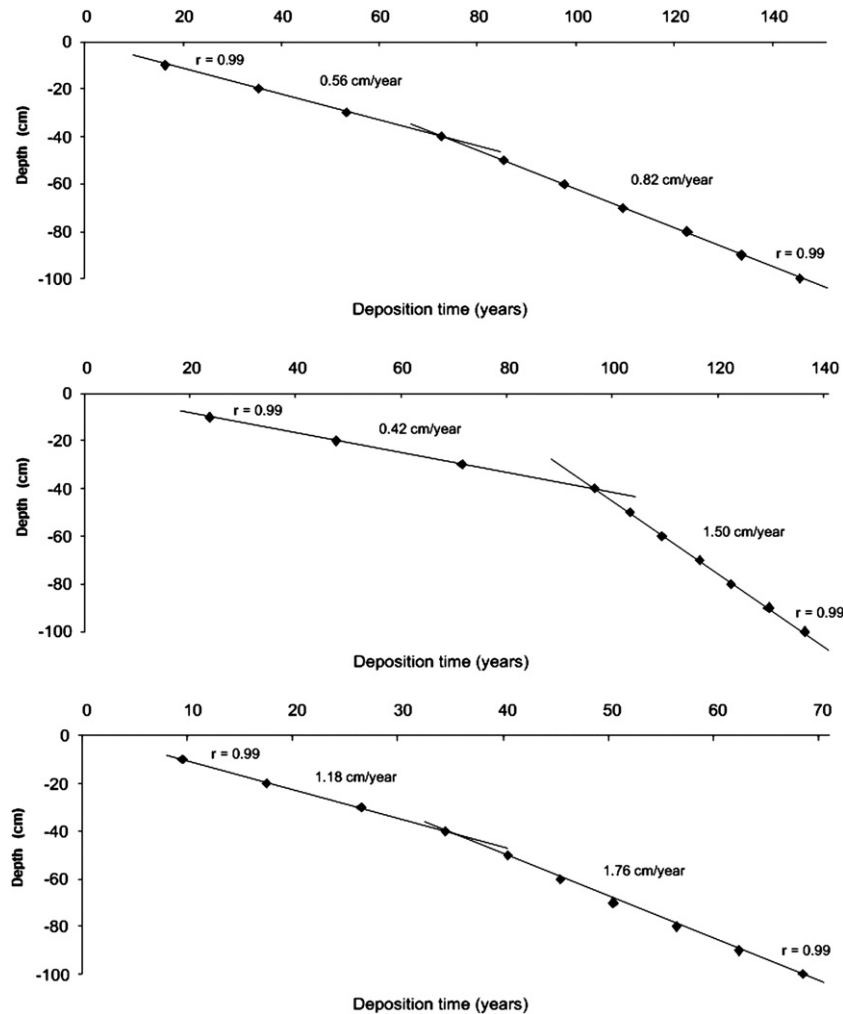


Fig. 9. Depth vs. deposition time relationships in sediment cores AMZ-1 (top), AMZ-2 (middle) and AMZ-3 (bottom) at Amazon River mouth, Amapá State, Brazil.

One striking aspect of all cores analyzed in this paper is that the mass accumulation rates (Fig. 8) and linear sedimentation rates (Fig. 9) were higher in the deeper portion of the profiles, in spite of the distance among them. Several factors have been pointed out for explaining the controlling mechanisms of the ^{210}Pb cyclicity, abrupt breaks in ^{210}Pb activity and nearly-uniform excess ^{210}Pb (Dukat and Kuehl, 1995; Jaeger and Nittrouer, 1995; Kuehl et al., 1995, 1996): grain-size variation associated with interbedding, presence of erosional surface, organic-carbon content, small-scale slumping and other mass-wasting processes, seaward transport and accumulation of low-activity fluid muds from the topset regions, intense biological reworking of sediments, physical reworking of the sediments, rapid (possibly episodic) deposition of sediment, and seasonal sediments resuspension from the inner shelf surface layer. A combination of some of these processes may be responsible for the breaks in ^{210}Pb activities despite can be related to major factors affecting the dynamics of the ocean waters.

Hydrographic observations in the South Atlantic have been historically fewer than in the North Atlantic, although it is particularly important as a region where oceanic properties are exchanged, mixed, and redistributed between different ocean basins, and it is unique as the only major ocean basin that transports heat from the poles toward the equator (Dong et al., 2009).

The earth's largest oceanic rings are formed by the retroflecting North Brazil Current (NBC) near 8°N in the western tropical

Atlantic. The NBC flows northward across the equator and pass the Amazon River mouth, entraining river-influenced shelf water along its nearshore edge (Fratantoni and Glickson, 2002; Field, 2005). This region is dominated by large anticyclonic rings shed at the retroflexion of the North Equatorial Counter Current (NECC) and the NBC, which then move northwestward along the South American coast (Jochum and Malanotte-Rizzoli, 2003). Therefore, these rings entrain water masses from the southern hemisphere and often, in their peripheral waters, water from the Amazon River (Fratantoni and Glickson, 2002). On the average, NBC rings form 5–6 times per year, propagate at a range of 8–30 km/day, have a radius on the order of 100–200 km, each ring transporting about 1 Sv ($=10^6 \text{ m}^3/\text{s}$) of water (Johns et al., 1990; Goni and Johns, 2001).

The NBC rings have received increasing attention since the mechanisms governing their generation, detachment and propagation pose a very interesting dynamical problem and also because the NBC rings may constitute an important component of the upper limb return flow of the Meridional Overturning Circulation (MOC) by contributing to the northward transport of southern Atlantic water into the northern subtropical gyre (Jochum and Malanotte-Rizzoli, 2003). In recent years, great interest has been aroused in monitoring the Atlantic Meridional Overturning Circulation (AMOC) due to its link to the past abrupt climate change and anthropogenic climate forcing (Dong et al., 2009; Zhang and McPhaden, 2009).

Table 5
Comparison of the mass accumulation rates determined in this paper with other values reported elsewhere.

Site	Locality	Reference	Mass accumulation rate (mg cm ⁻² yr ⁻¹)
Amisk Lake	Alberta, Canada	Turner and Delorme (1996)	20
Elkwater Lake	Alberta, Canada	Turner and Delorme (1996)	270
Birchbark Lake	Saskatchewan, Canada	Turner and Delorme (1996)	10
Clearwater Lake	Saskatchewan, Canada	Turner and Delorme (1996)	260
Gillis Lake	Saskatchewan, Canada	Turner and Delorme (1996)	40
Chapala Lake	Guadalajara, Mexico	Fernex et al. (2001)	440 and 620
Navarro de Andrade Lake	Rio Claro city, São Paulo St., Brazil	Bonotto et al. (2005)	752
Ibitinga Creek	Rio Claro city, São Paulo St., Brazil	Bonotto et al. (2005)	1014
Claro Stream	Rio Claro city, São Paulo St., Brazil	Bonotto et al. (2005)	406
Corumbataí River (upper course)	Ajapi city, São Paulo St., Brazil	Bonotto and Lima (2006)	802
Corumbataí River (lower course)	Piracicaba city, São Paulo St., Brazil	Bonotto and Lima (2006)	224
Itapetinga Creek (middle course)	Atibaia city, São Paulo St., Brazil	Sabaris and Bonotto (2010)	782
Itapetinga Creek (lower course)	Atibaia city, São Paulo St., Brazil	Sabaris and Bonotto (2010)	48
Porcos Creek	Atibaia city, São Paulo St., Brazil	Sabaris and Bonotto (2010)	170
Onofre Creek	Atibaia city, São Paulo St., Brazil	Sabaris and Bonotto (2010)	758
Atibaia River	Atibaia city, São Paulo St., Brazil	Sabaris and Bonotto (2010)	262
Folha Larga Creek (middle course)	Atibaia city, São Paulo St., Brazil	Sabaris and Bonotto (2010)	488
Folha Larga Creek (lower course)	Atibaia city, São Paulo St., Brazil	Sabaris and Bonotto (2010)	531
Caetetuba Stream (lower course)	Atibaia city, São Paulo St., Brazil	Sabaris and Bonotto (2010)	394
Caetetuba Stream (upper course)	Atibaia city, São Paulo St., Brazil	Sabaris and Bonotto (2010)	761
Curuai Great Lake	Óbidos, Pará St., Brazil	Moreira-Turcq et al. (2004)	420
Curuai Great Lake	Óbidos, Pará St., Brazil	Moreira-Turcq et al. (2004)	1160
Curuai Great Lake	Óbidos, Pará St., Brazil	Moreira-Turcq et al. (2004)	1100
Araçá Lake	Porto Velho city, Rondônia St., Brazil	Vergotti (2008)	2256
Tucunaré Lake	Porto Velho city, Rondônia St., Brazil	Vergotti (2008)	489
Paca Lake	Porto Velho city, Rondônia St., Brazil	Vergotti (2008)	1189
Nazaré Lake	Porto Velho city, Rondônia St., Brazil	Vergotti (2008)	187
Demarcação Lake	Porto Velho city, Rondônia St., Brazil	Vergotti (2008)	611
Santa Catarina Lake	Porto Velho city, Rondônia St., Brazil	Vergotti (2008)	1749
Brasileira Lake	Porto Velho city, Rondônia St., Brazil	Vergotti (2008)	989
Conceição Lake	Porto Velho city, Rondônia St., Brazil	Vergotti (2008)	599 and 2256
Samuel Hydropower Lake	Porto Velho city, Rondônia St., Brazil	Vergotti (2008)	509
Amazon River Mouth (profile AMZ-1)	Macapá city, Amapá St., Brazil	This paper	720 and 1090
Amazon River Mouth (profile AMZ-2)	Macapá city, Amapá St., Brazil	This paper	450 and 1950
Amazon River Mouth (profile AMZ-3)	Macapá city, Amapá St., Brazil	This paper	1730 and 2510

Zhang and McPhaden (2009) utilized 5-decades of historical hydrographic data to estimate transport variability in NBC that is a western boundary choke point of the AMOC in the tropical South Atlantic. Their results revealed a large magnitude NBC transport variations on multi-decadal time scales and also that the NBC is coherent with the Atlantic Multi-decadal Oscillation in sea surface temperature, multi-decadal swings in Sahel drought, Atlantic hurricane activity and the subtropical and subpolar upper ocean salinity anomalies. Zhang and McPhaden (2009) used the Accumulated Cyclone Energy (ACE) index as a measure of the Atlantic hurricane activity and found that the transport time series of the NBC at 6°S is significantly correlated with both the Atlantic ACE and the detrended Sahel rainfall at zero lag, indicating that decadal changes of Atlantic hurricane activity and Sahel rainfall are part of the atmospheric response to the AMOC multi-decadal variation in the tropical Atlantic.

According to Zhang and McPhaden (2009), the maximum ACE index from the early 1970s to the 1990s was 90 and the data plotted in Fig. 9 for profile AMZ-3 indicates in this period a linear sedimentation rate equal 1.18 cm yr⁻¹. On the other hand, the ACE index increased up to about 130 in the 1960s (Zhang and McPhaden, 2009), whereas the linear sedimentation rate in profile AMZ-3 also raised (1.76 cm yr⁻¹, Fig. 9). Therefore, it is plausible admit that the Atlantic hurricane activity also affects the sedimentation rates in the area studied, i.e. when it increases (higher ACE index), the sediments deposition also increases, as expected. Such relationship could explain the major breaks in the ²¹⁰Pb activity observed in cores AMZ-1, AMZ-2 and AMZ-3. Zhang and McPhaden (2009) reported 5-decades of historical hydrographic data that is a period compatible with the sediments deposition time found in profile AMZ-3.

Unfortunately, there is a lack of historical hydrographic data extending back in the past up to the epochs related to cores AMZ-1 and AMZ-2 that exhibit lower sedimentation rates. This certainly could expand the relationship to others areas and would strengthen the interpretation of the signatures evidenced in core AMZ-3.

5. Conclusion

Estuaries and the lands surrounding them are places of transition from land to sea, and are formed when freshwater from rivers and streams meet and mix with salt water from the ocean. Estuarine environments are among the most productive on earth, creating more organic matter each year than comparably sized areas of forest, grassland, or agricultural land. Many different habitat types are found in and around estuaries, including shallow open waters, freshwater and salt marshes, swamps, sandy beaches, mud and sand flats, rocky shores, oyster reefs, mangrove forests, river deltas, tidal pools, and sea grasses. The productivity and variety of estuarine habitats foster an accentuated abundance and diversity of wildlife. Thousands of species of birds, mammals, fish, and other wildlife depend on estuarine habitats as places to live, feed, and reproduce. And many marine organisms, including most commercially important species of fish, depend on estuaries at some point during their development. However, the formation of estuarine environments is greatly dependent of the sedimentation rates and the results of this study indicated that some anthropogenic influences can be evaluated from their values. The sedimentation rates in the near-surface sediments layers at Amazon River mouth was determined for three profiles and ranged from 450 mg cm⁻² yr⁻¹ (0.42 cm yr⁻¹) to 2510 mg cm⁻² yr⁻¹

(1.76 cm yr⁻¹). The adoption of the steady-state condition requested by the application of the ²¹⁰Pb method implied on the occurrence of abrupt jumps in which the mass accumulation rates and the linear sedimentation rates were higher in the deeper portion of the profiles, in spite of the distance among them. The strong fluctuations verified ~ 50 cm depth in profile AMZ-3 for the concentrations of SiO₂, Al₂O₃, K₂O, CaO, MgO, P₂O₅, Fe₂O₃ and MnO is compatible with the occurrence of anthropogenic inputs coupled to the mining activities involving Mn ores at Serra do Navio in Amapá State. Such finding is confirmed by the presence of enhanced dissolved sulfate and bicarbonate contents in interstitial waters of the same profile. The Atlantic hurricane activity appeared to affect the sedimentation rates in the area studied since its increase indicated by the higher Accumulated Cyclone Energy index is correlated with a more accentuated sediments deposition. The results here reported also permit a wide spectrum of future investigations to be held in the area studied, as can develop new frontiers toward deeper investigations focusing the theme, aiding important information on others anthropogenic processes taking place there, for instance, opening of artificial channels to a better access to remote areas and implications of the very common bulls activities conducted in the region or further applications of the ²¹⁰Pb activities on the study of the dynamics of the ocean waters at that highly energetic environment.

Acknowledgments

CNPq (National Council for Scientific and Technologic Development) in Brazil is greatly thanked for financial support of this investigation. Two anonymous referees are greatly thanked by critics and suggestions on the previous versions of the manuscript.

References

- Allison, M.A., Nittrouer, C.A., Faria Jr., L.E.C., 1995. Rates and mechanisms of shoreline progradation and retreat downdrift of the Amazon River mouth. *Mar. Geol.* 125, 373–392.
- APHA (American Public Health Association), 1989. Standard Methods for the Examination of Water and Wastewater, seventeenth ed. APHA, Washington, DC.
- Appleby, P.G., Oldfield, F., 1978. The calculation of ²¹⁰Pb dates assuming a constant rate of supply of unsupported ²¹⁰Pb to the sediment. *Catena* 5, 1–8.
- Appleby, P.G., Oldfield, F., 1992. Application of lead-210 to sedimentation studies. In: Ivanovich, M., Harmon, R.S. (Eds.), *Uranium Series Disequilibrium: Applications to Environmental Problems*, second ed. Clarendon Press, Oxford, pp. 731–778.
- Argollo, R.M., 2001. Chronology of the recent sedimentation and deposition of heavy metals at Baía de Todos os Santos using Pb-210 and Cs-137. PhD Thesis, Universidade Federal da Bahia, Salvador, 104 pp.
- Bárbara, V.F., da Cunha, A.C., de Siqueira, E.Q., 2005. Análise da qualidade das águas do Rio Araguaí (AP) utilizando o sistema de modelagem Qual2E. In: CD-ROM Proc. CONPEEX – Congresso de Pesquisa, Ensino e Extensão, Universidade Federal de Goiás, Goiânia, pp. 1–3.
- Baskaran, M., Naidu, A.S., 1995. ²¹⁰Pb-derived chronology and the fluxes of ²¹⁰Pb and ¹³⁷Cs isotopes into continental shelf sediments, East Chukchi Sea, Alaskan Arctic. *Geochim. Cosmochim. Acta* 59 (21), 4435–4448.
- Bonotto, D.M., Andrews, J.N., 1997. The implications of the laboratory Rn-222 flux measurements to the radioactivity in groundwaters: the case of a karstic limestone aquifer. *Appl. Geochem.* 12 (6), 715–726.
- Bonotto, D.M., Andrews, J.N., 1999. Transfer of radon and parent nuclides ²³⁸U and ²³⁴U from soils of Mendip Hills area, England, to the water phase. *J. Geochem. Explor.* 66, 255–268.
- Bonotto, D.M., Caprioglio, L., 2002. Radon in groundwaters from Guarany aquifer, South America: environmental and exploration implications. *Appl. Radiat. Isot.* 57, 931–940.
- Bonotto, D.M., Lima, J.L.N., 2006. ²¹⁰Pb-derived chronology in sediment cores evidencing the anthropogenic occupation history at Corumbataí river basin, Brazil. *Environ. Geol.* 50 (4), 595–611.
- Bonotto, D.M., Almeida, K.Y.M., Sieber, S.S., 2005. Sedimentation rates in the Corumbataí river basin, Brazil, derived from ²¹⁰Pb measurements. In: Des Walling, E., Horowitz, A.J. (Eds.), *Sediment Budget*, first ed., vol. 1. IAHS Press, Wallingford, pp. 294–302.
- Brandini, F., 2005. Mar dulce mar. Amigos da terra – Amazônia Brasileira. http://www.amazonia.org.br/opiniaio/artigo_detail.cfm?id=166380.
- DeMaster, D.J., Kuehl, S.A., Nittrouer, C.A., 1986. Effects of suspended sediments on geochemical processes near the mouth of the Amazon River: examination of biological silica uptake and the fate of particle reactive elements. *Cont. Shelf Res.* 6, 107–125.
- Dominguez, C., 2004. Importance of rivers for the transportation system of the Amazon. In: Aragón, L.E., Clusener-Godt, M. (Eds.), *Issues of Local and Global Use of Water from the Amazon*. UNESCO, Montevideo, pp. 77–100.
- Dong, S., Garzoli, S., Baringer, M., Meinen, C., Goni, G., 2009. Interannual variations in the Atlantic meridional overturning circulation and its relationship with the net northward heat transport in the South Atlantic. *Geophys. Res. Lett.* 36 (L20606), 1–5.
- Drummond, J.A., Pereira, M.A.P., 2007. O Amapá nos tempos do manganês: um estudo sobre o desenvolvimento de um estado amazônico 1943–2000. Garamond, Rio de Janeiro, 172 pp.
- Duarte, C.R., Bonotto, D.M., 2000. Calibração em energia e concentração de espectrômetro gama para análise de U, Th e K. *Geociências* 19 (2), 313–319.
- Dukat, D.A., Kuehl, S.A., 1995. Non-steady-state ²¹⁰Pb flux and the use of ²²⁸Ra/²²⁶Ra as a geochronometer on the Amazon continental shelf. *Mar. Geol.* 125, 329–350.
- Faure, G., 1991. Principles and Applications of Inorganic Geochemistry. MacMillan Publishing Co., New York, 626 pp.
- Fernex, F., Valle, P.Z., Sanchez, H.R., Michaud, F., Parron, P., Dalmasso, J., Funel, G.B., Arroyo, M.G., 2001. Sedimentation rates in Lake Chapala (Western Mexico): possible active tectonic control. *Chem. Geol.* 177, 213–228.
- Ffield, A., 2005. North Brazil current rings viewed by TRMM Microwave Imager SST and the influence of the Amazon Plume. *Deep-Sea Res.* 52 (Pt. 1), 137–160.
- Flynn, W.W., 1968. The determination of low levels of polonium-210 in environmental materials. *Anal. Chim. Acta* 43, 221–227.
- Fratantoni, D.M., Glickson, D.A., 2002. North Brazil current generation and evolution observed with SeaWiFS. *J. Phys. Oceanogr.* 32, 1058–1074.
- Furch, K., 1984. Water chemistry of the Amazon basin: the distribution of chemical elements among fresh waters. In: Sioli, H. (Ed.), *The Amazon – Limnology and Landscape Ecology of a Mighty Tropical River and Its Basin*. Springer, Dordrecht, pp. 167–200.
- Furch, K., Junk, W.J., 1997. Physicochemical conditions in the floodplains. In: Junk, W.J. (Ed.), *The Central Amazon floodplain – Ecology of a Pulsing System*. Springer Verlag, Heidelberg, pp. 69–108.
- Godoy, J.M., Moreira, L., Wanderley, C., Mendes, L.B., Bragança, M.J., 1998. A study of Guanabara bay sedimentation rates. *J. Rad. Nu. Chem.* 227 (1–2), 157–160.
- Goldich, S.S., 1938. A study in rock weathering. *J. Geol.* 46, 17–58.
- Goni, G.J., Johns, W.E., 2001. A census of North Brazil Current rings observed from TOPEX/POSEIDON altimetry: 1992–1998. *Geophys. Res. Lett.* 28 (1), 1–4.
- Hach, 1992. *Water Analysis Handbook*, second ed. Hach Co., Loveland, 831 pp.
- IBGE (Instituto Brasileiro de Geografia e Estatística), 2007. O censo do Brasil. <http://www.sidra.ibge.gov.br>.
- Jaeger, J.M., Nittrouer, C.A., 1995. Tidal controls on the formation of fine-scale sedimentary strata near the Amazon River mouth. *Mar. Geol.* 125, 259–281.
- Jochum, M., Malanotte-Rizzoli, P., 2003. On the generation of North Brazil current rings. *J. Mar. Res.* 61 (2), 147–173.
- Johns, W.E., Lee, T.N., Schott, F.A., Zantopp, R.J., Evans, R.H., 1990. The North Brazil current retroflection: seasonal structure and eddy variability. *J. Geophys. Res.* 95 (C12), 22103–22120.
- Kiehl, E.J., 1977. Interpretation of Soil Properties. Teaching Text. ESALQ (University of Agriculture “Luiz de Queirós”, USP-University of São Paulo), Piracicaba, 237 pp.
- Kineke, G.C., Sternberg, R.W., 1995. Distribution of fluid muds on the Amazon continental shelf. *Mar. Geol.* 125, 193–233.
- Kuehl, S.A., Pacioni, T.D., Rine, J.M., 1995. Seabed dynamics of the inner Amazon continental shelf: temporal and spatial variability of surficial strata. *Mar. Geol.* 125, 283–302.
- Kuehl, S.A., Nittrouer, C.A., Allison, M.A., Faria, L.E.C., Dukat, D.A., Jaeger, J.M., Pacioni, T.D., Figueiredo, A.G., Underkoffler, E.C., 1996. Sediment deposition, accumulation, and seabed dynamics in an energetic fine-grained coastal environment. *Cont. Shelf Res.* 16 (5/6), 787–815.
- Moore, W.S., Astwood, H., Lindstrom, C., 1995. Radium isotopes in coastal waters on the Amazon shelf. *Geochim. Cosmochim. Acta* 59 (20), 4285–4298.
- Moore, W.S., DeMaster, D.J., Smoak, J.M., McKee, B.A., Swarzenski, P.W., 1996. Radionuclide tracers of sediment–water interactions on the Amazon shelf. *Cont. Shelf Res.* 16 (5/6), 645–665.
- Moreira-Turcq, P.M., Jouanneau, J.M., Turck, B., Seyler, P., Weber, O., Guyot, J.L., 2004. Carbon sedimentation at Lago Grande de Curuai, a floodplain lake in the low Amazon region: in situ sedimentation rates. *Palaeogeogr. Palaeoclimatol.* 214 (1–2), 27–40.
- Munsell, 1975. *Soil Color Charts*. Macbeth, Baltimore.
- Nittrouer, C.A., Kuehl, S.A., Sternberg, R.W., Figueiredo Jr., A.G., Faria, L.E.C., 1995. An introduction to the geological significance of sediment transport and accumulation on the Amazon continental shelf. *Mar. Geol.* 125, 177–192.
- Nittrouer, C.A., Kuehl, S.A., Figueiredo Jr., A.G., Allison, M.A., Sommerfield, C.K., Rine, J.M., Faria, L.E.C., Silveira, O.M., 1996. The geological record preserved by Amazon shelf sedimentation. *Cont. Shelf Res.* 16 (5/6), 817–841.
- Piper, A.M., 1944. A graphic procedure in the geochemical interpretation of water-analyses. *Eos Trans. AGU* 25, 914–928.
- Ravichandran, M., Baskaran, M., Santschi, P.H., Bianchi, T.S., 1995. Geochronology of sediments in the Sabine–Neches estuary, Texas, U.S.A. *Chem. Geol.* 125, 291–306.
- Sabaris, T.P.P., Bonotto, D.M., 2010. Sedimentation rates in Atibaia River basin, São Paulo State, Brazil, using ²¹⁰Pb as geochronometer. *Appl. Radiat. Isot.* doi:10.1016/j.apradiso.2010.08.016.
- Scarpelli, W., 2006. Arsenio do minério de manganês de Serra do Navio. *Novos Cadernos NAEA* 6 (1), 101–133.

- Silveira, O.F.M., 1998. A Planície Costeira do Amapá: Dinâmica de Ambiente Costeiro influenciado por grandes fontes fluviais quaternárias. PhD Thesis, Universidade Federal do Pará, Belém, 198 pp.
- Sioli, H., 1950. Das wasser im Amazonasgebiet. *Forsch. Fortschr.* 26, 274–280.
- Smoak, J.M., DeMaster, D.J., Kuehl, S.A., Pope, R.H., McKee, B.A., 1996. The behavior of particle-reactive tracers in a high turbidity environment: ^{234}Th and ^{210}Pb on the Amazon continental shelf. *Geochim. Cosmochim. Acta* 60 (12), 2123–2137.
- Turner, L.J., Delorme, L.D., 1996. Assessment of ^{210}Pb data from Canadian lakes using the CIC and CRS models. *Environ. Geol.* 28, 78–87.
- Udden, J.A., 1898. Mechanical Composition of Wind Deposits. In: Augustana Library Publ., vol. 1, pp. 1–69.
- Vergotti, M., 2008. Use of ^{210}Pb to study the mercury deposition in lakes from Madeira River basin (RO). PhD Thesis, UNESP-Universidade Estadual Paulista, Rio Claro, 126 pp.
- Wanty, R.B., Lawrence, E.P., Gundersen, L.C.S., 1992. A theoretical model for the flux of radon from rock to groundwater. In: Gates, A.E., Gundersen, L.C.S. (Eds.), *Geologic Controls on Radon*. *Geol. Soc. Am.*, vol. 271, pp. 73–78.
- Wentworth, C.K., 1922. A scale of grade and class terms for clastic sediments. *J. Geol.* 30, 377–392.
- Zhang, D., McPhaden, M.J., 2009. Multidecadal variability of the North Brazil current. *Geophys. Res. Abstr.* 11 (EGU2009–2595), 1.